7

Heubeck, C., K. Story, P. Peng, C. Sullivan, and S. Duff, 2004, An integrated reservoir study of the Liuhua 11-1 field using a high-resolution three-dimensional seismic data set, *in* Seismic imaging of carbonate reservoirs and systems: AAPG Memoir 81, p. 149–168.

An Integrated Reservoir Study of the Liuhua 11-1 Field Using a High-Resolution Three-Dimensional Seismic Data Set

Christoph Heubeck
Department of Geosciences, Freie Universität Berlin, Berlin, Germany

Kenneth Story
DDD Energy, Houston, Texas, U.S.A.

Pat Peng
BP, Houston, Texas, U.S.A.

Claire Sullivan
BP, Houston, Texas, U.S.A.

Stuart Duff
Independent contractor, Wellington, New Zealand

ABSTRACT

Liuhua 11-1 field, located in the Pearl River Mouth Basin offshore south China, consists of diagenetically altered Miocene limestone comprising a shallow-water carbonate bank. This bank forms the topmost and youngest interval of a larger, extensively karsted, buried carbonate platform. A three-dimensional (3-D) seismic survey of Liuhua field yielded a very high-resolution data set (>200 Hz), allowing a spatial resolution less than 5 m. This data set was subsequently used to produce a reservoir model that closely linked petrophysical, log, and seismic data.

The carbonate stratigraphy suggests several subaerial exposure events that significantly modify primary stratification of the carbonate bank through diagenesis. These include freshwater leaching, burial compaction, cementation, and late diagenetic flushing of the bank. The combined diagenetic changes had three principal effects: (1) exacerbation of primary facies-dependent differences in porosity through a series of dissolution-reprecipitation steps; (2) widespread incipient carbonate collapse at or below the scale of seismic resolution; and (3) formation of numerous regionally occurring karst sinkholes of as much as 400 m diameter shortly before final drowning of the

platform. Incipient collapse of the friable carbonate framework is expressed seismically by a reduction in amplitude.

Carbonate dissolution appears to be ongoing because sagging continues to affect all strata overlying the reservoir to the seafloor. Subsurface dissolution may be a result of either flushing of the carbonate platform by cold, undersaturated marine waters or may be a result of active biodegradation of the hydrocarbons along the oil-water contact and the concomitant release of acids.

INTRODUCTION

The Pearl River Mouth Basin forms the passive Atlantic-type margin of south China related to the Tertiary opening of the South China Sea (Fulthorpe and Schlanger, 1989; Dorobek, 1997). In this basin, a geographically restricted carbonate platform formed on top of the subsiding Dongsha horst block during rifting of the South China Sea in the middle Miocene (Figure 1). The topmost, geographically most restrictive, and youngest part of this platform now forms an elevated horst block containing the Liuhua 11-1 field (Christian and Tyrrell, 1991; Erlich et al., 1990; Moldovanyi et al., 1995; Turner and Hu, 1990, 1991; Turner, 1990; Tyrrell and Christian, 1992). The reservoir is comprised of middle Miocene bioclastic rhodolith packstones and foram-algal grainstones of the Zhujiang Formation. They overlie fluviodeltaic sandstones and shales of the Miocene Zhuhai Formation, which, in turn, unconformably overlie granitic basement of the Dongsha block (Figure 2). The carbonate bank (Zhujiang Formation) is sharply overlain by more than 1000 m of Miocene–Holocene marine shales of the Hanjiang Formation across a flooding surface. This flooding surface was described as an example of a ''drowning unconformity'' by Erlich et al. (1990, 1991), Tyrrell and Christian (1992), and Erlich et al. (1993).

The reservoir, containing approximately 1.3 BBOIP, produces biodegraded, 16–22° API oil from shallow depths with a very strong bottom-water drive. The

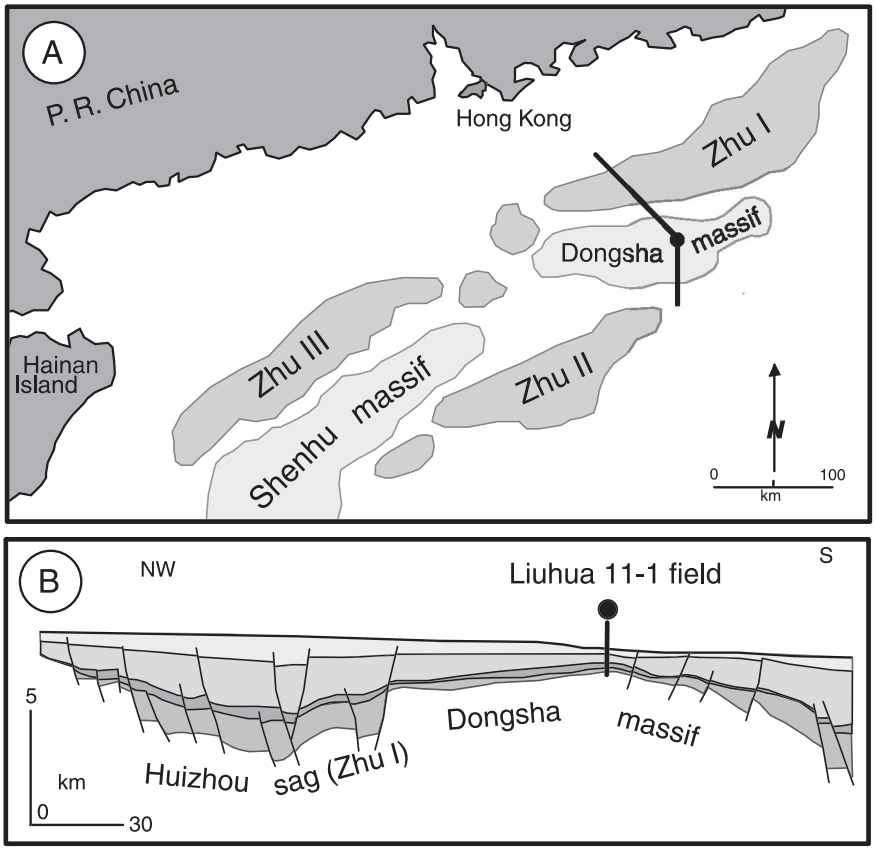

FIGURE 1. (A) Basin map of Pearl River Mouth Basin. Liuhua field is located approximately 210 km southeast of Hong Kong in a water depth of 300 m in platform carbonates that formed in the structurally highest part of the Dongsha horst block during Miocene rifting of the South China Sea between the Zhu I and Zhu II turbidite-filled basins. (B) Schematic regional geologic cross section. Modified from Tyrrell and Christian (1992).

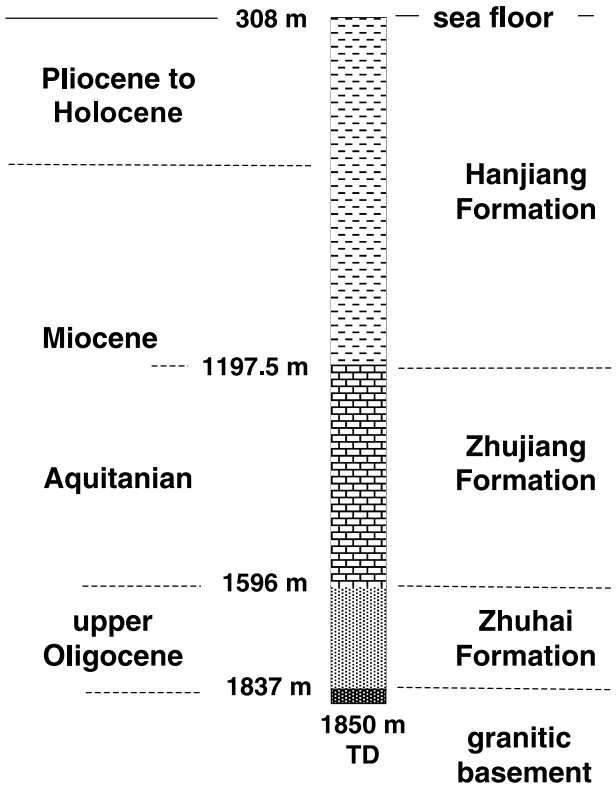

FIGURE 2. Stratigraphic column encountered in well LH 11-1-1A, the discovery well for the Liuhua field (modified after Tyrrell and Christian, 1992). The sedimentary sequence overlying the crystalline basement of the Dongsha horst block is a typical rift-drift sequence of increasing water depth. The fluviodeltaic deposits of the Zhuhai Formation are overlain by Miocene platform carbonates of the Zhujiang Formation whose upper part contains the Liuhua reservoir. The Zhujiang Formation is, in turn, unconformably overlain by deep-marine shales of the Hanjiang Formation. TD = total depth.

combination of heavy oil, shallow reservoir, and strong water drive requires the accurate placement of horizontal production wells.

This chapter describes the principal insights gained from the high-resolution seismic survey over Liuhua field into distribution and origins of reservoir heterogeneity through the integration of geophysical, geological, and petrophysical data, thereby allowing insights in subaerial and subsurface karst processes on field scale. It also briefly describes the construction of a reservoir model from the seismic data through integration of production data from wells with petrophysical parameters from core and logs, visualization, and finally reservoir modeling, including predictive flow simulation.

RESERVOIR GEOLOGY

Field History, Depositional Environment, and Diagenesis

The Liuhua 11-1 field is located 210 km southeast of Hong Kong in a water depth of approximately 300 m (Figure 1). It was discovered by Amoco in January 1987. Significant technical challenges to field development included the water depth, its location in the ''typhoon alley,'' and the presence of heavy oil in a large but shallow and relatively thin reservoir interval with a very strong bottom-water drive. Several geologic aspects of Liuhua and the Dongsha horst have been described in detail in previous publications, including its regional setting and exploration history (Tyrrell and Christian, 1992; Wu et al., 1997), its stratigraphy and karst features from seismic data (Moldovanyi et al., 1995), and the drowning of the carbonate platform (Erlich et al., 1990). Field development was authorized in March 1993 and production from the first of a total of 25 horizontal extended-reach wells started in March 1996 (Gu and Ye, 1992). To optimize production through the quantification of reservoir compartmentalization and heterogeneity, a three-dimensional (3-D) survey was acquired over the field in July 1997. Geologic and seismic acquisition parameters enabled the acquisition of an extremely high resolution seismic data set.

The field is a combination stratigraphic-structural trap in which the primary carbonate bank buildup formed on a structural high. Continued faulting and gentle anticlinal folding of the bank provided a secondary trapping mechanism after deposition of the Hanjiang Shale seal.

Although the bioclastic grainstones and packstones had excellent primary intergranular porosity, most of the reservoir porosity is diagenetic in origin. Petrographic and isotopic data from Liuhua cores indicate that the reservoir potential of Zhujiang carbonates has been modified (from oldest to youngest) by the following processes (Boutell and Moldovanyi, 1992; Moldovanyi et al., 1995; Wagner et al., 1995):

1) Repeated subaerial exposure of the upper part of the carbonate bank and leaching of metastable grains by meteoric waters (James and Choquette, 1990)
2) Corresponding precipitation of calcite cement at various levels near the paleo-ground water table
3) Selective brecciation of low-strength intervals resulting from compaction
4) Postburial leaching, particularly of coarse-grained, high-porosity intervals of sufficient mechanical

Table 1. Sequence of diagenetic events affecting the reservoir of Liuhua field.

Event number (earliest to latest)	*Diagenetic event*	*Impact on porosity development*
1	Subaerial exposure; leaching of metastable grains by meteoric water	⇑
2	Precipitation of calcite cement at various levels near the paleoground water table	⇓⇓
3	Brecciation of low-strength intervals resulting from compaction	⇓⇓
4	Postburial leaching, particularly of coarse-grained, high-porosity intervals of sufficient mechanical strength	⇑⇑
5	Solution compaction, affecting primarily fine-grained intervals	⇓⇓
6	Burial cementation by equant calcite spar	⇓
7	Mechanical compaction affecting primarily intervals of lower strengths	⇓
8	Leaching by compaction water and fluids	⇑⇑⇑

strength, such as red algal boundstones, by cold, undersaturated marine waters

5) Solution compaction affecting primarily fine-grained intervals
6) Burial cementation by equant calcite spar
7) Mechanical compaction affecting primarily intervals of lower strengths
8) Leaching by compaction water and fluids

The effects of these processes varied through time (Table 1). Some processes, such as meteoric leaching, were most important during marine and shallow burial diagenesis, whereas others, such as solution compaction and compaction-water leaching, became more important during later stages of burial and may be active even today. The reservoir is free of dolomite and of terrigenous input, such as clay minerals, based on log evaluation and core data. This monomineralic $CaCO_3$ composition facilitated seismic interpretation and petrophysical modeling.

As a result of the extensive diagenetic overprint, low-porosity, highly cemented (''tight'') streaks of occur commonly within the Liuhua reservoir. They are laterally extensive, but not contiguous. Core inspection, petrography, and log analysis of these zones show that their thickness ranges from a few centimeters to a few tens of meters. Turner and Hu (1991) and Moldovanyi et al. (1995) describe their petrographic and isotopic characteristics in detail. These authors (as well as P. Wagner, 1995, personal communication) conclude that the low-porosity zones are principally the result of several events of subaerial exposure of the carbonate bank and precipitation of dissolved calcite by meteoric fluids near the water table and were accentuated by subsequent diagenetic events.

The principal low-porosity zones are sufficiently continuous, thick, or well-cemented to affect fluid flow through the reservoir and are, in part, above the seismic resolution of approximately 4 m. Therefore, they can be characterized in the 3-D reservoir description and the numerical reservoir model. The low-porosity zones have a double effect on well productivity: They protect the wellbore from early water breakthrough and reduce pressure support from the strong bottom-water drive. Consequently, development wells drilled into a high-porosity lower zone with only a moderately tight subjacent zone had very high productivity but watered out rapidly.

Reservoir Stratigraphy

Seismic stratigraphy of the Liuhua bank shows evidence of being predominantly primary in some places and predominantly diagenetic in origin in others. Core inspection and thin-section petrography show that the reservoir stratigraphy on a seismic scale is a result of postdepositional (i.e., diagenetic) porosity enhancements and reductions; however, the cores also show that these diagenetic changes follow primary grain-size differences and therefore outline primary depositional facies. Seismic stratification appears to outline primary depositional features, such as mounds, bank fronts, and platform flats (Figure 4). We therefore postulate that most porosity stratification in Liuhua field represents actual time surfaces that bound depositional units (Moldovanyi et al., 1995), representing a diagenetic enhancement of an original facies-dependent primary stratigraphy.

The detailed reservoir stratigraphy of Liuhua field has been outlined, based on the largely cored discovery and appraisal wells, by Tyrrell and Christian (1992) and Moldovanyi et al. (1995) and will not be repeated here. Wagner et al. (1995) described its petrographic and isotopic composition. The stratigraphic description below essentially confirms these descriptions but adds additional detail gained through the drilling and geologic interpretation of the development wells (Stark, 1991; Heubeck, 1998).

Liuhua field comprises (from top to bottom) the following units (Figures 3, 4):

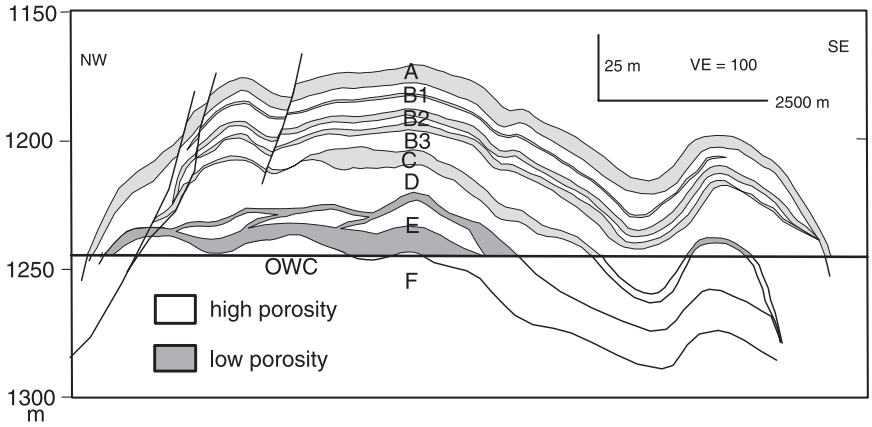

FIGURE 3. Simplified geologic cross section across Liuhua field. The stratigraphic architecture of Liuhua 11-1 field alternates between thin zones of high and low porosity with varying degrees of fieldwide continuity. These variations constitute largely highly varying degrees of cementation, but may also, in part, accentuate primary fabric and grain-size variation of the different facies in the carbonate bank depositional environment. Note the high vertical exaggeration (VE). OWC = oil-water contact.

- The A Zone, uppermost unit of the Zhujiang Formation on the Liuhua structure, is dominantly a firm rhodolith-foraminifera packstone approximately 4.3–5.5 m thick, infiltrated by marine clays. Porosity is mostly interskeletal and averages about 13%. The A Zone is overlain by a thin, discontinuous glauconitic sand at the base of the overlying Hanjiang Formation that buried the drowned bank.
- The B1 Zone is a firm, friable rhodolith-foraminiferal packstone, 7.9–8.5 m thick (Figure 3). Bioclastic and skeletal material include algae, calcareous benthonic foraminifera, and indeterminate skeletal material that possibly includes bryozoans, coral fragments, and radiolaria. Intraskeletal and framework porosity ranges between 25 and 33%. This unit is the uppermost high-porosity zone within the reservoir. Extensive development drilling in this zone showed that a 1- to 1.5-m-thick ''lower''-porosity (17–24%) streak (termed the *B12 subzone*) occurs at a fixed position within the B1 Zone throughout the development area. This slightly more cemented streak serves as an excellent marker during directional drilling operations.
- The B2 Zone is approximately 13.7 m thick and lithologically identical to the B1 Zone but is generally more cemented by opaque calcite cement (Figures 3, 5). In comparison to the B1 Zone, voids, cavities, and spaces in the B2 Zone are greatly reduced in size and frequency. This zone is highly stratified internally with seven alternating high- (16–24%) and low- (6–12%) porosity streaks, each about 0.3–2.5 m thick. Thickness and porosity values of these streaks are consistent throughout the 2- × 4-km area accessed by the development wells. Therefore, the detailed stratification within the B2 Zone, expressed in porosity logs of individual wellbores, can be readily correlated across the field.
- The B3 Zone, approximately 9 m thick, is lithologically similar to the B1 Zone but shows even higher visual and log porosity, ranging from 23 to 34%. Moldic, interskeletal, and intraskeletal porosity are common. A single development well drilled into this zone reached high productivity, probably because of better pressure support from the water leg, but watered out quickly.
- The C Zone is predominantly a milky white foraminiferal-skeletal packstone, tightly cemented by white opaque calcite, with only minor visual porosity in cuttings and core (Figure 5). Fracture porosity, however, is common. The C Zone is the principal ''tight'' zone within the reservoir. On 3-D seismic data, the C Zone grades from a strong and continuous seismic reflector on the west side of the field with approximately 14% log-calculated porosity in a seismically discontinuous, 6-m-thick unit of approximately 27% porosity to the east. No development well has penetrated the C Zone or any of the underlying zones.
- The D Zone was penetrated only twice by appraisal wells. It appears internally complex on seismic (Figures 3, 4) but is overall a high-porosity zone with a mean log porosity 28%. Low-porosity streaks within the D Zone are visible on seismic sections. These may outline possible depositional mounds.
- The E Zone forms a low-porosity zone of foraminiferal packstone, approximately 17 m thick, at the base of the oil-filled reservoir. The low porosity may be a result of calcite cementation along the former oil-water contact (OWC) by degradation of oil by oxygen-rich water. Its average porosity is 16% but varies widely. Subsequent deformation caused the E Zone to bend into a very open anticline. At the bank margins, the E Zone dips below the OWC. It is, therefore, not effective in protecting overlying oil and horizontal wellbores from water coning.
- The F Zone is a highly porous zone of leached, friable skeletal packstone and grainstone below the OWC. Interpretation of core texture and thin

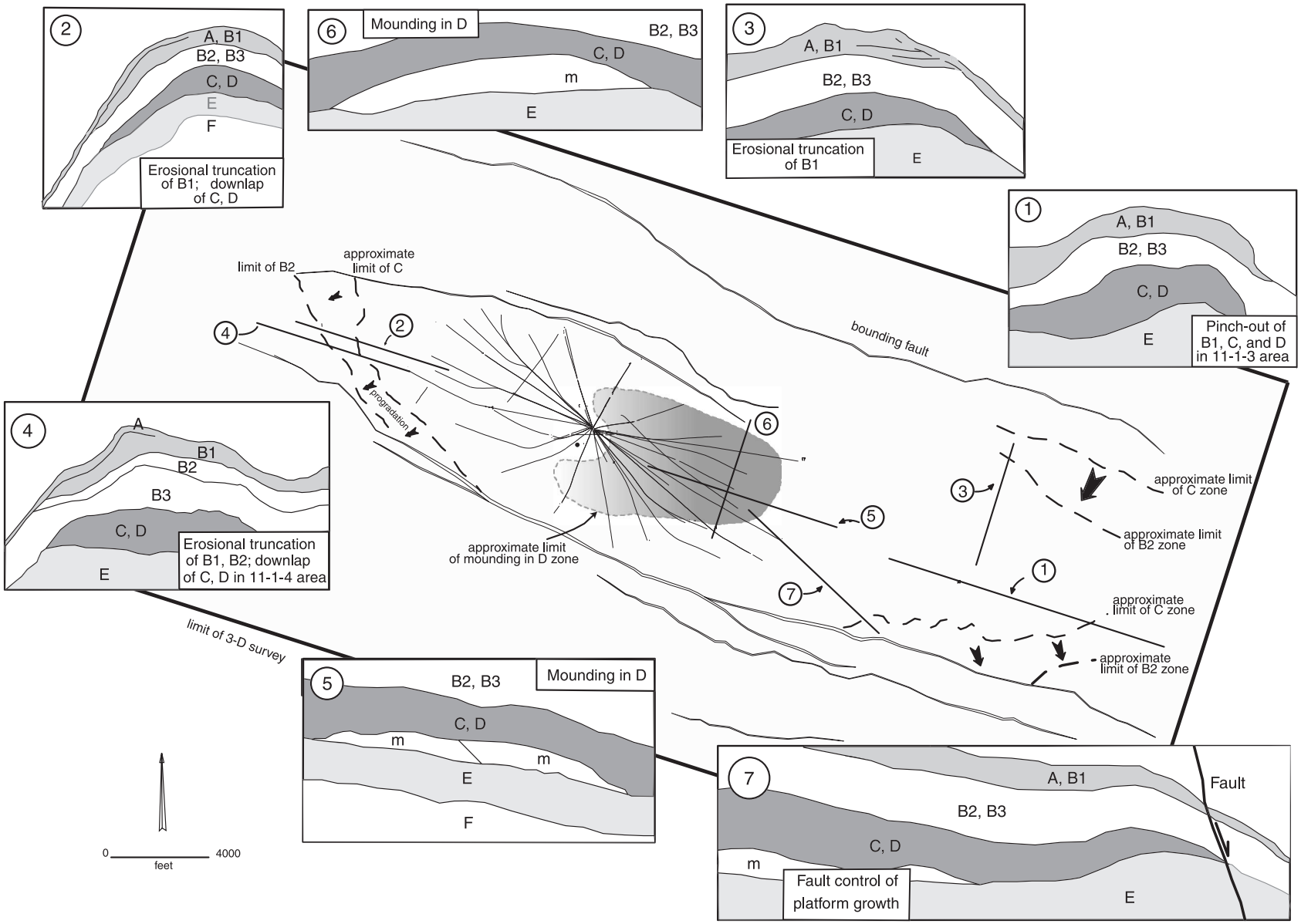

FIGURE 4. Liuhua bank stratigraphic architecture from 3-D seismic data, based on selected seismic sections through parts of the field. Central map shows area of 3-D survey, location of faults bounding the platform, development wells, and profiles 1 through 7 (numbered insets) taken from seismic time sections. These insets show suspected mounding in the D Zone and limited seaward (southward) progradation of the bank margin in its upper part (B and C Zones).

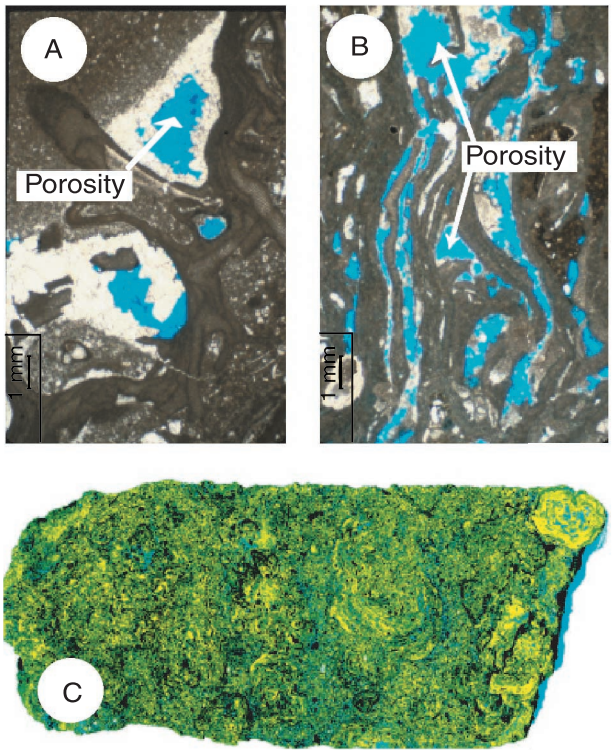

FIGURE 5. Thin-section photomicrographs and core slabs of the Zhujiang Formation in Liuhua field. (A) Thin section showing vuggy and moldic porosity in the well-cemented, low-porosity C Zone. (B) Algal boundstone from the high-porosity B2 subzone showing interskeletal porosity. (C) False-color core-slab photograph showing friable rhodolith packstone, also from the high-porosity B2 Zone. Core width is approximately 12 cm.

sections suggests that this zone was exposed to flushing by cold seawater undersaturated with respect to $CaCO_3$, whereas the strong water drive implies that this flushing may extend to the present.

SEISMIC GEOPHYSICS

Rationale for Three-Dimensional Seismic Data

Development wells had delivered an abundance of information about the composition, structure, and fine-scale stratigraphy of the A, B1, B2, and B3 Zones. Well production data, however, had made it clear that individual well performance was also strongly affected by the continuity, permeability, and stratigraphy of the zones underlying the producing sections of the wellbores (Figures 3, 4). Little was known about these zones aside from the partially cored appraisal wells and the two-dimensional (2-D) seismic lines, thus preventing proper estimates about expected well productivity and risk of premature water coning. Seismic source and acquisition parameter modeling and testing on a reprocessed 2-D line suggested that a 3-D survey could clarify internal reservoir heterogeneity to a high degree and identify high-porosity well targets.

Seismic Acquisition and Inversion

The seismic acquisition was conducted during calm seas with short 1500-m streamers and shallow 3.5-m-tow depths. The 180-Hz field data, enhanced during processing, produced peak frequencies of 240 Hz. Temporal and spatial resolution of this data set is approximately 4 m; detectability is about 1.5 m. Approximately 4 million traces were processed at a bin spacing of 5 × 5 m over a 100-km^2 area (Figure 6).

Seismic stratigraphy and wellbore data were used to constrain an acoustic impedance inversion of the time data. Because the relationship of acoustic impedance to core porosity is nearly linear for Liuhua, because of the monomineralic mineralogy of the reservoir limestone, fieldwide acoustic impedance was readily calculated, converted to porosity through a quadratic regression equation related to core-plug data, and matched to core-calibrated log data from the vertical wells penetrating the reservoir. Ultimately, petrophysical data and modeling coupled with the seismic inversion were used together to create a spatial distribution of porosity, permeability, and saturation.

Seismic Interpretation

Interpretation of the regional 2-D seismic data has identified the sequence-stratigraphic framework of the Dongsha Platform and recognized the regional distribution of (poorly resolved) karst features (Moldovanyi et al., 1995). Over the bank buildup of Liuhua field, another 2-D seismic survey, spaced 2 and 1 km apart, has identified the general reservoir architecture of the field and recognized its problematic stratigraphic heterogeneity (Moldovanyi et al., 1995). The newly acquired 3-D data offered the opportunity to greatly expand the level of detail in the structural and stratigraphic interpretation. The interpretation focused on (1) quantifying the relative contributions of stratigraphic trapping vs. folding, faulting, and fracturing in trap definition; (2) the influence of damage halos near the bounding faults in constraining productive wellbore lengths; (3) which ''major'' faults penetrated the reservoir to the OWC and served as conduits for water coning and which ''minor'' faults did not; and (4) the impact of karst collapse structures on reservoir hydraulics and field development.

Five stratigraphic tops (A, B2, C, E, and F) and the principal bounding faults of the Liuhua horst block

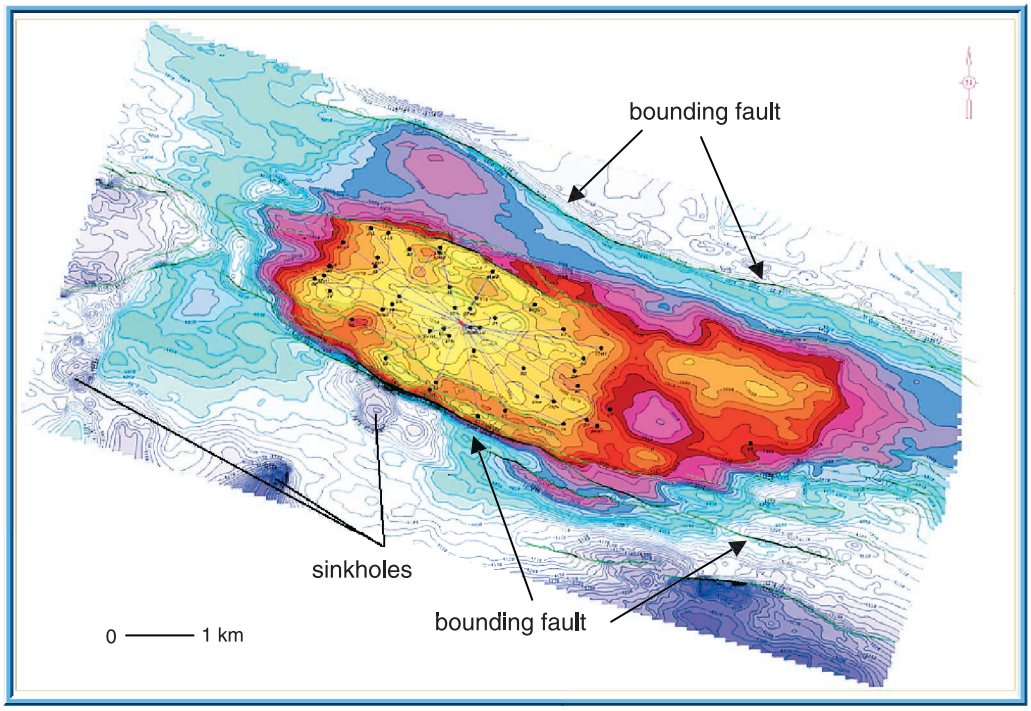

FIGURE 6. Depth-structure map for the top of the Liuhua carbonate platform, also top of the reservoir (top of zone A). Development wells are shown as thin black lines, extending from the platform at the central and structurally highest part of the carbonate bank. Note the west-northwest–east-southeast–striking faults bounding the horst structure and large several circular depressions interpreted as carbonate-collapse features (karst-related sinkholes) just to the southwest of the field.

were mapped on the seismic data set. Structural interpretation grouped structural elements into one of five classes: bounding faults, major faults, minor faults, chaotic zones, and gas sag margins. The depth structure map for the top unit of the carbonate complex (the Top A surface) is shown in Figure 6.

The Liuhua horst block between the major bounding faults is gently folded into a broad, northwest-southeast–trending, doubly plunging anticline (Figure 7). Total relief on this anticline at the top of the reservoir between the top of the bounding faults and the structural crest is approximately 11 m over a distance

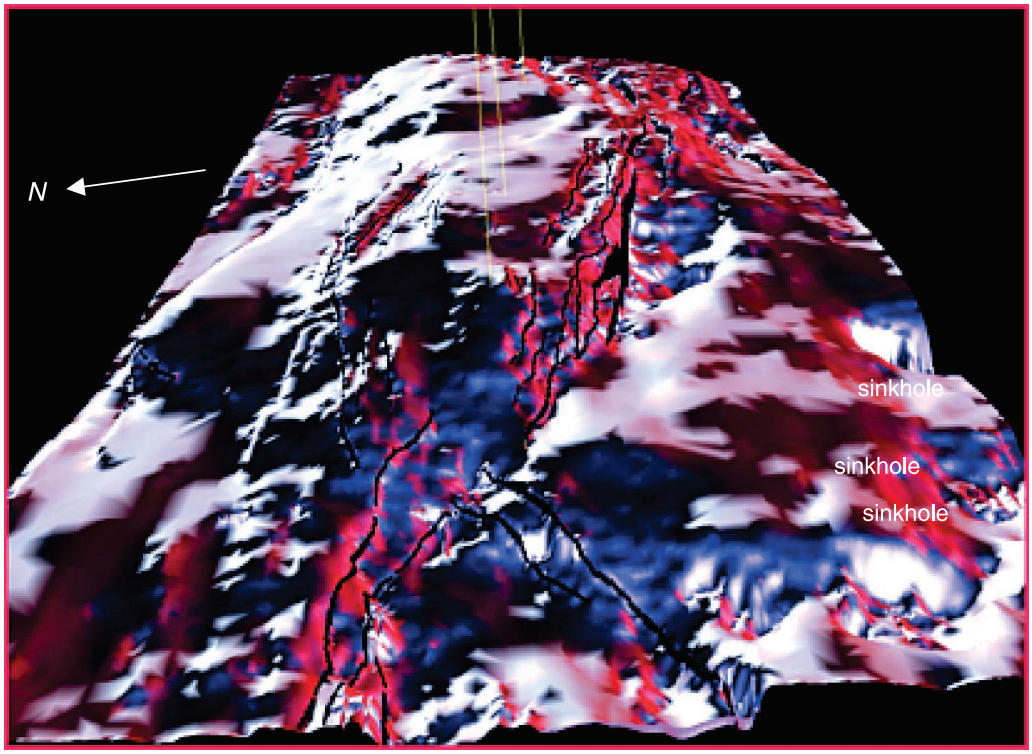

FIGURE 7. Perspective view of the same surface as in Figure 6, the top surface of the reservoir. View is from the northwest along the long axis of the gently folded and moderately faulted Liuhua horst block. Vertical yellow lines show wellbore traces of the wells LH 11-1-4 (foreground, appraisal), LH 11-1-1A (middle ground, discovery well), and LH 11-1-3 (background, appraisal). Several karst sinkholes are partly or completely imaged in the right foreground. Vertical exaggeration = 20.

of approximately 1.2 km. Maximum relief between the structural crest and either down-plunge end of the anticline is approximately 75 m over a distance of 5 km. The maximum elevation difference between the OWC and the crest of the structure is also 75 m.

Bathymetric relief between bank edge and top, associated with original deposition, was probably on the order of approximately 10 m, judged by the bank-margin depositional geometry, the lack of cut-and-fill features throughout, and the uniformity of primary stratification across the bank interior (Figures 3, 4). Facies changes related to present-day structural elevation are not apparent. Therefore, much of the Liuhua folding was probably postdepositional and was probably closely related to the major faulting along the bounding faults near the bank margin. Only some faulting near the bank edge appears to affect zone thicknesses and was, therefore, pre- or syndepositional, at least in part.

Two groups of ''bounding faults'' on the north and south sides of the Liuhua reservoir delimit the production area, defining an intervening horst block. Maximum dip-slip displacement on the southern and northern bounding faults is 49 and 24 m, respectively. Displacement diminishes along strike because of transfer to subsidiary faults and folds and because of minor changes in strike. In seismic cross sections, the bounding faults can be traced from crystalline basement to the seafloor, which is blanketed by Holocene sediments (Figure 8). The bounding faults may, therefore, still be active. ''Gas sags'' on seismic time sections occur along strike on both bounding faults. Damage halos associated with bounding faults are approximately 300 m wide on the southern fault but distinctly narrower on the northern bounding faults, possibly because of the reduced offset. Within each damage halo, subsidiary normal faults with offsets generally less than 5 m parallel the bounding faults.

Several ''major faults'' penetrate the reservoir to the aquifer. The faults typically show a minimum dip-slip displacement of 5 m in their midsection and extend for greater than 300 m in map view. These faults are water conduits and must be strictly avoided by the wellbores. The common ''minor faults'' represent in part en echelon–stepping segments of suspected strike-slip fault zones. Several wellbore trajectories penetrated minor faults (Figure 10) but minor evidence of faulting was found in only one well log. Individual well productivity does not appear to be adversely affected by penetration of minor faults.

''Chaotic zones'' of seismic time sections are zones of diminished and discontinuous amplitude reflectivity and low, distributed coherence in the individual low-porosity zones B2, C, and E. No chaotic zone was cored in Liuhua but several of these zones were penetrated by production wells. Cuttings and well logs through these zones showed no deviation from their appearance in other wellbores. The ''chaotic zones'' are likely zones of stratigraphic brecciation resulting from carbonate dissolution and probably serve as major channels for water coning toward the production wellbores.

''Gas sags'' appear as continuous, straight, or curved zones of low coherency. They appear downfaulted on seismic time sections (Figure 9). However, direct evidence from logs and drill-bit cuttings shows that these seismic discontinuities are artifacts caused by an abrupt lateral variation of seismic traveltime and are not, or only to a minor degree, caused by actual structural displacement. Because seismic reflectors appear offset on seismic time-domain sections, the resulting amplitude discontinuity is computed as a zone of low coherence and resembles a fault on a coherence map (Figure 10).

Conventional structural fracturing appears to be unimportant on a fieldwide scale and therefore for reservoir flow simulation studies in Liuhua. Microfracturing, however, may be more significant. Two production wells were logged by microfracture logging tools but showed only a few hairline cracks along with one open and one closed (cemented) fracture each.

Karst Features

Moldovanyi et al. (1995) correctly interpreted the ''hummocky seismic facies'' at the top of the Zhujiang Limestone on the regional 2-D seismic lines across the Dongsha Platform as a regional extensive karst field of individual and nested sinkholes (dolines). Of the region surveyed by 2-D seismic, seven large and many small sinkholes fall within the area of the 3-D survey; in addition, the high resolution of the seismic data allows the interpretation of other karst-related features that will be discussed below.

The sinkholes are imaged best with a coherency map at the top of the reservoir (Figure 10). They are typically 100 to approximately 500 m across and show a relief of as much as 15 m. Similar karst sinkholes associated with former sea level lowstands are common features on modern reefs and carbonate banks, e.g., in the Bahamas and Belize (Gascoyne et al., 1979; Mylroie and Carew, 1995) and in the Maldives (Purdy and Bertram, 1993); they are commonly known as ''blue holes.'' Their surface expression is circular because of the dissolution over a cave system at depth and cave-ceiling collapse. Karst dissolution features may form particularly early in regions of tropical cyclone activity (Bourrouilh, 1998). In cross section (Figures 8, 11, 12), at least two additional observations can be made: (1) columns of low amplitude exist within and above the collapse zones and also near the bounding faults; they extend to the sea floor; and (2) concentric structural sag above

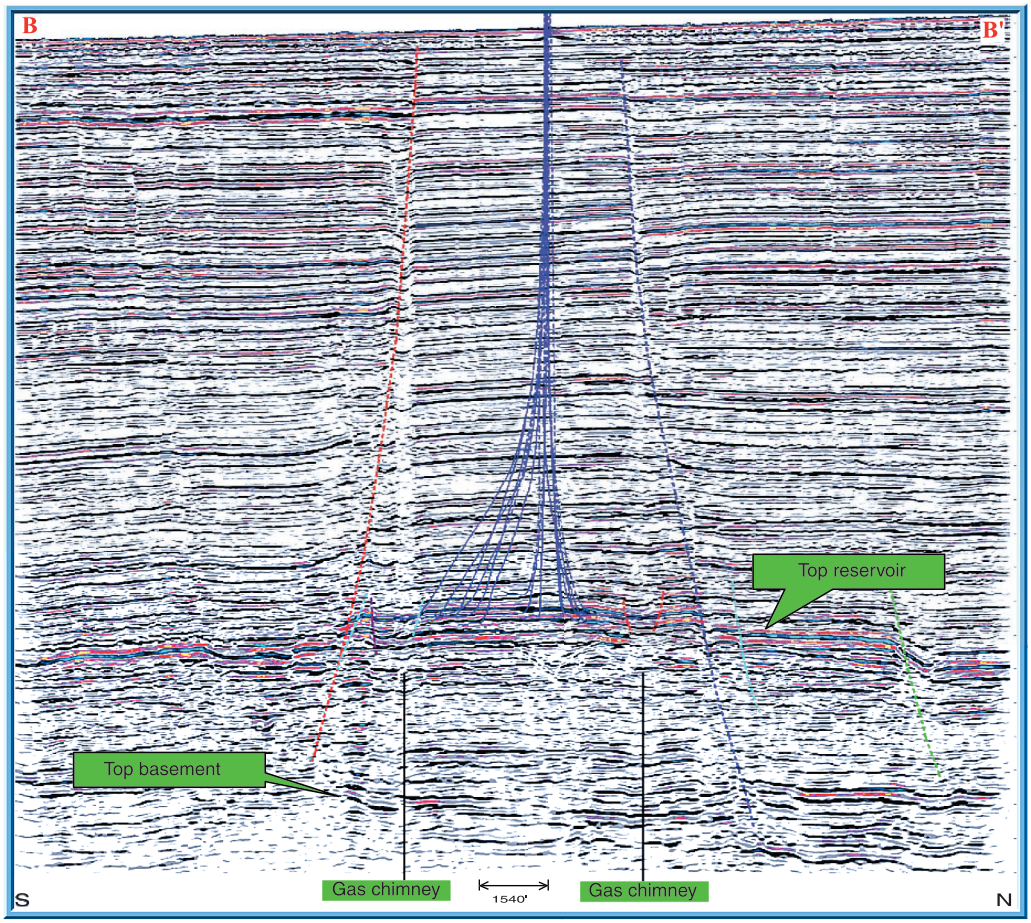

FIGURE 8. Seismic time section BB′ (for location, see Figure 10) across Liuhua field. Bounding faults can be traced from well below the reservoir nearly to the sea floor, possibly also offsetting Holocene sediments, and suggest that the bounding faults may still be active. Two gas chimneys emanating from the reservoir are imaged as diffuse vertical zones of reduced amplitude and time sag.

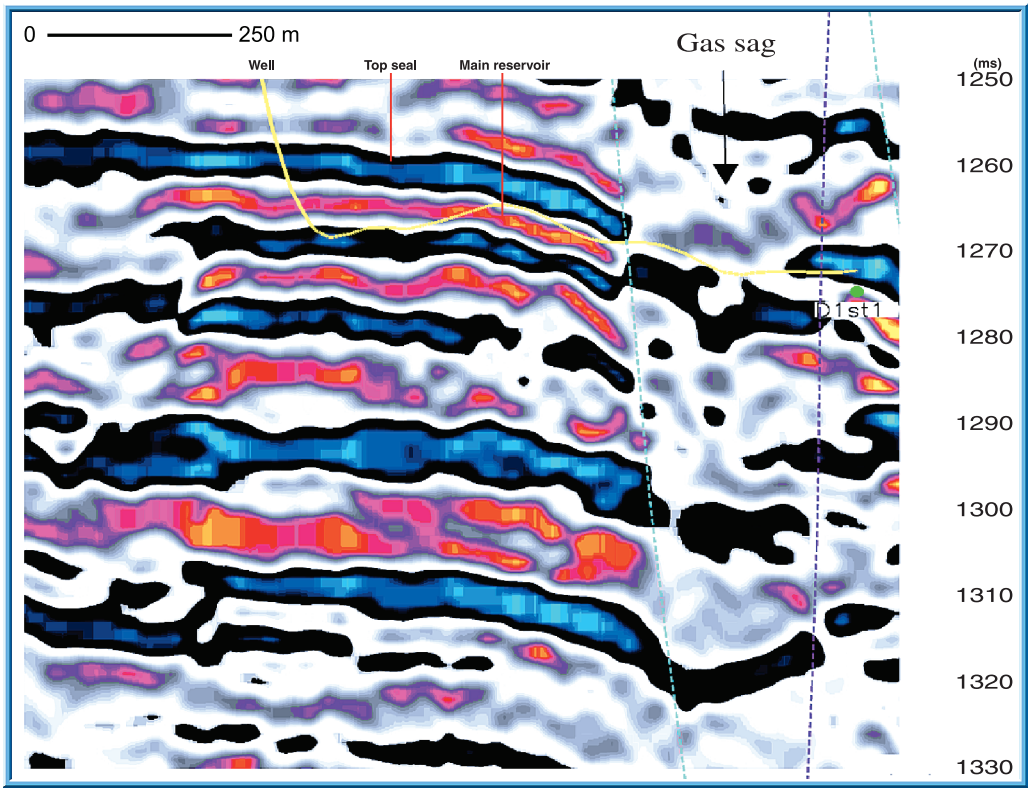

FIGURE 9. Detail of "gas sag" at the top of the reservoir in seismic time section. Gas sag is imaged through reduced amplitude and a laterally sharply defined zone of seismic sag, thus resembling a structural graben. The wellbore (thin yellow line) crossing the time sag, however, drilled continuously within the B Zone of reservoir, without showing evidence of any structural offset. Horizontal width of image is approximately 2 km. Vertical scale: 1 ms ≈ 2 m.

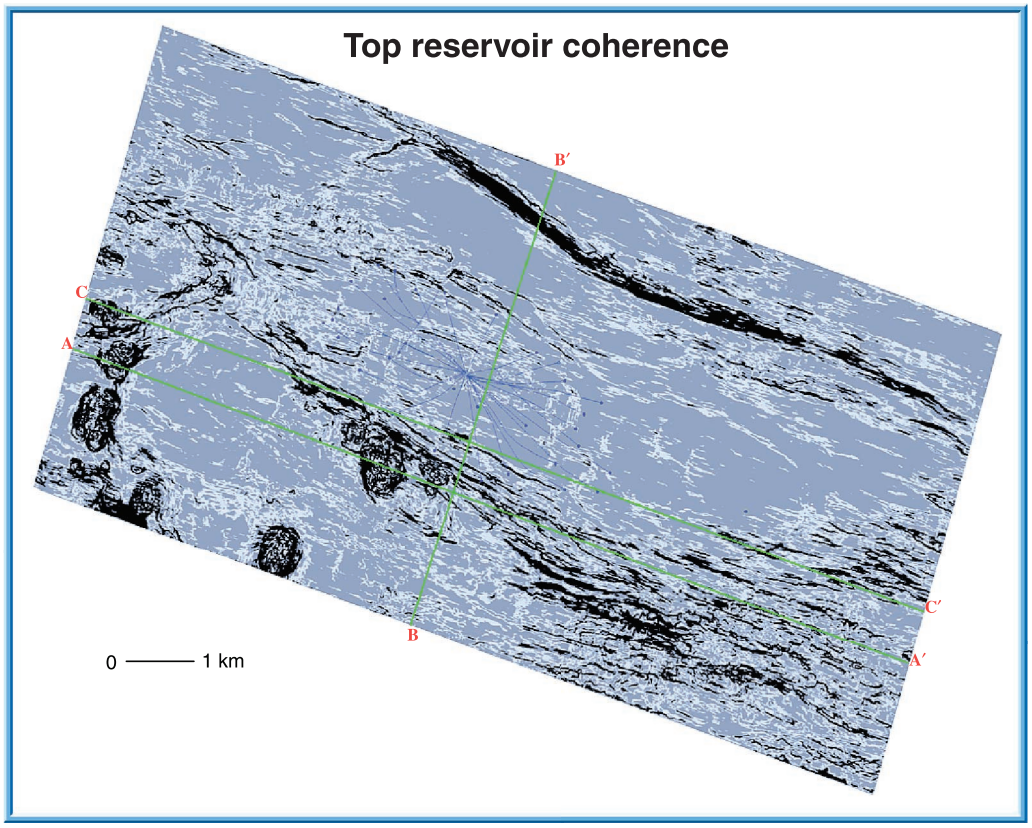

FIGURE 10. Seismic map of the top of the reservoir showing coherence attribute over the survey area of approximately 7 × 12 km. Traces of horizontal wellbores are shown in blue. Notice cluster of circular, partly intersecting sinkholes to the southwest of the reservoir, in part associated with fault zones bounding the reservoir. Cross section AA′ is shown in Figure 12, cross section BB′ is shown in Figure 8, and cross section CC′ is shown in Figure 11.

the collapse zones affects the entire overburden. The east-west seismic section in Figure 12 demonstrates these characteristics over the large sinkhole along the southern fault margin. Apparently, a gas-generating process is occurring near the base of the reservoir level; the upward migration of gas is facilitated by the sinkhole. We believe that the apparently active subsurface limestone dissolution, the associated discrete and diffuse carbonate collapse, and gas-chimney formation are related and can be attributed to either or both of two processes: (1) ongoing biodegradation of the oil and related release of acids or (2) continued flushing of the Dongsha Platform by cold marine waters undersaturated with respect to $CaCO_3$.

The first alternative, termed *oil-field karst*, has been proposed for various worldwide examples (Hill, 1992, 1995). In the case of the Liuhua reservoir, bacteria at the OWC may decompose hydrocarbon into carbon dioxide, methane, and hydrogen sulfide. CO_2 released into the seawater forms carbonic acid and dissolves the carbonate substrate, causing sagging and collapse in the overlying strata. Methane, hydrogen sulfide, excess carbon dioxide, and a large amount of water rise up along the bounding and major faults and through the collapse pipes and leave behind an amplitude dim zone in the microfractured marine shale associated with the gas chimneys. The telltale signs of inactive oil-field karst, gypsum, however, have not been reported from Liuhua cores. It is possible that it may have been dissolved.

Alternatively, cold marine waters may also contribute to carbonate dissolution. The Zhuhai sandstone aquifer, underlying the Zhujiang Limestone, crops out on the seafloor at the fault-bounded edge of the Dongsha Platform, resulting in a strong bottom-water drive. The chalky, highly porous, and leached texture of the reservoir F Zone below the OWC testifies that carbonate dissolution was active in the past. In what may have been the first step in a two-stage process, compaction-water leaching may have also initially contributed to the alteration of the F Zone by moving water vertically downward, then horizontally outward.

From a field-production standpoint, the ongoing solution collapse is important in that it will create vertical zones for water encroachment both outside of and within the productive area of the reservoir. Zones of reduced reflection strength (“dim zones”) not only overlie clearly collapsed, typically circular off-structure sinkholes, but are also associated with subtle fracture swarms paralleling the bounding faults within the reservoir. These smaller features are generally only faintly visible on the coherency map (Figure 10). There are also nonlinear partial-dissolution features that are not completely collapsed into cylindrical patterns. Only the irregular edges of some of these features are discernible

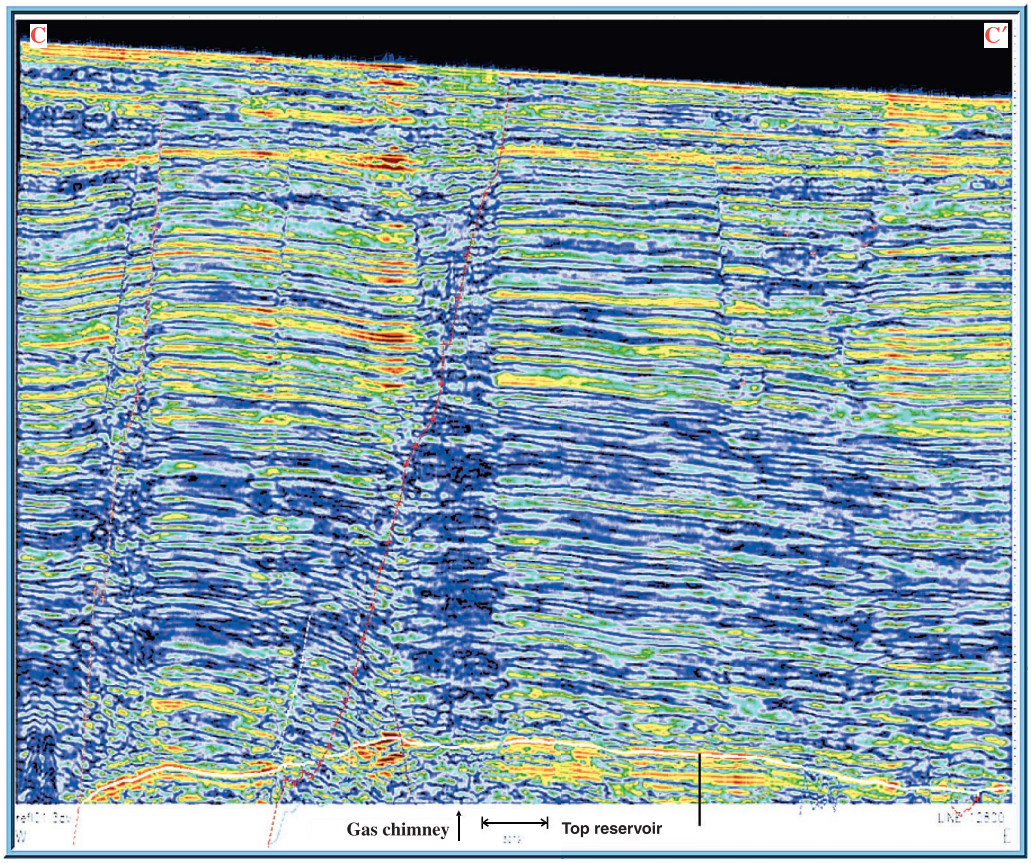

FIGURE 11. Seismic time section CC′ along strike of the Liuhua horst block, crossing the Liuhua field slightly off-center. Width of image is approximately 12 km. Top of the reservoir is shown as the gently anticlinally folded and faulted bright reflector near the bottom of the image. This section obliquely crosses a zone of gas sag presumably related to minor and diffuse faulting in the central, structurally flat part of the reservoir, and is associated with a major gas chimney represented by a column of low amplitude (see Figure 10 for location). High amplitudes next to this gas chimney but well above the reservoir may be escaped gas, charging turbiditic sandstones of Pliocene–Pleistocene age.

(Figure 10). Several isolated, partial-dissolution ''dimples'' that are suspected to exist within the core producing area are associated with these subtle attribute irregularities.

Core description can only partially confirm the widespread evidence of various degrees of exposure from seismic data. The principal geologic evidence for repeated exposure events derives from thin section petrography (meniscus cements, early moldic porosity; Wagner et al., 1995) and oxygen-isotope stratigraphy on the Liuhua cores (Boutell and Moldovanyi, 1992) that indicate a vadose zone diagenetic environment and a periodic influence of meteoric water. However, there is a lack of macroscopic diagnostic fabrics, such as collapse breccias (McMechan et al., 1998; Loucks, 1999), pink or laminated cave-fill facies (Cocozza and Gandin, 1990), radial fibrous or blocky calcite, tension cracks and fissures, or chaotic stratigraphy (Kerans, 1988), that are typical characteristics of karsted reservoirs and which would fill a ''mesoscale'' data gap between the microscopic petrographic data and the macroscopic seismic evidence for exposure and karsting. The lack of exposure-diagnostic mesoscopic fabrics is largely because of the fact that production wellpaths were carefully designed to avoid apparently structured zones (because of the danger of early water coning) and zones of low porosity (because of the evident relationship with reduced production volumes). However, where amplitude ''dim zones'' were penetrated by an (uncored) development well, no unusual fabrics or lithologies were reported from cuttings descriptions either. Therefore, the features responsible for seismic amplitude reduction are probably at or below the seismic detection limit and are not evident in the cuttings; they may be brecciated areas of incipient carbonate collapse (''crackle breccia'' of Loucks, 1999). Production data suggest that the ''dim zones'' may be responsible for higher-than-expected water production from individual wells. The suspected microfracturing associated with both the major and incipient solution collapse was modeled successfully during the reservoir hydraulic simulation with local adjustments to the vertical water transmissibility.

Within the limits of the 3-D survey, the large sinkholes are preferentially associated with the subvertical bounding faults. The fact that karst processes were controlled by these faults suggests that these faults were major vertical fluid conduits already early in the diagenetic process and may have been a factor in bounding the extent of carbonate platform growth,

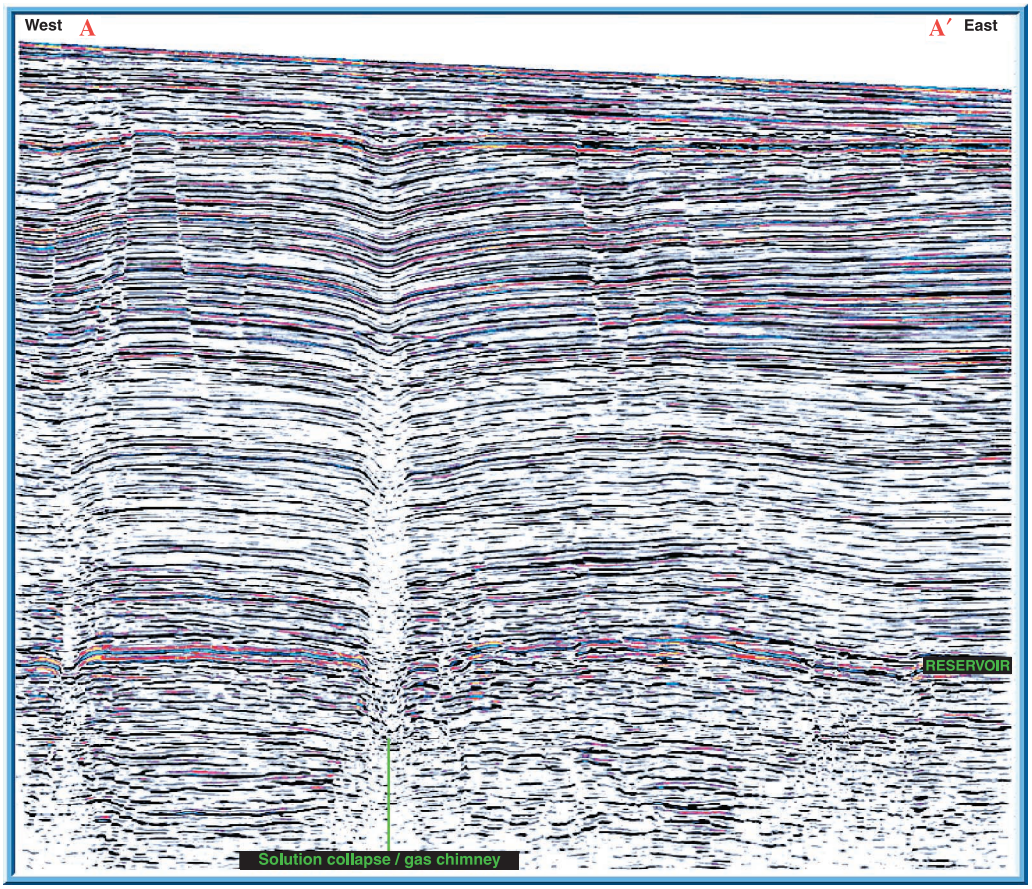

FIGURE 12. East-west–oriented seismic time cross section AA′, crossing the largest karst sinkhole of the 3-D survey, located just outside the major faults bounding of the development area. The concentric structural sag above the collapse zones affects the entire overburden.

similar to their distribution in the west Texas Yates field (Tinker and Hruk, 1995). While none of the large karst sinkholes are located within the development area, there does appear to be a strong relationship between the poor production of the western field area and the large sinkhole cluster along the southern bounding fault nearby (Figures 6, 10).

Porosity degradation in the western field area, suggested by a lack of contiguous acoustic resonance in the reef reservoir complex, can also be demonstrated in a spectral decomposition map (Figure 13). This frequency-analysis attribute indicates that the western area has poor acoustic values, that the core producing area has high values, and that the eastern, undeveloped area shows arcuate structures of alternating high and low values. Oils from the latter two reservoir segments also have a different composition and viscosity. This attribute can probably be interpreted as a measure of petrophysical matrix continuity, or coherence, in the frequency domain. The spectral decomposition values can be used to delineate zones of increasing matrix discontinuity that may either result from variable primary depositional patterns (e.g., carbonate facies of different water depths) and/or various degrees of carbonate dissolution and microfracturing.

Reservoir Characterization and Visualization

The objective of the reservoir characterization was to produce a detailed and accurate depth-converted porosity and permeability model of the reservoir useful for identification of contiguous high-porosity trends and for wellbore planning, history matching of producing wells, and predictive reservoir simulation. Nine additional surfaces from well control were added to the five surfaces picked from seismic control and interpreted using a sequence-stratigraphic framework to improve simulation resolution. The inversion values (porosity) range from 10 to 34% and demonstrate the spatial variability of the porosity zones (Figure 14).

The thin porosity layers in the reservoir and the localized effects of ''time sag'' in the solution collapse zones complicated the structural depth conversion of the model. Because the main producing zone averages only approximately 8 m in thickness (approximately 4 ms), the depth conversion required high precision to ensure that the 25 horizontal wellbores plotted in the correct reservoir zones as interpreted from logs. Log-calculated porosity data from vertical and horizontal wells showed an excellent agreement with the

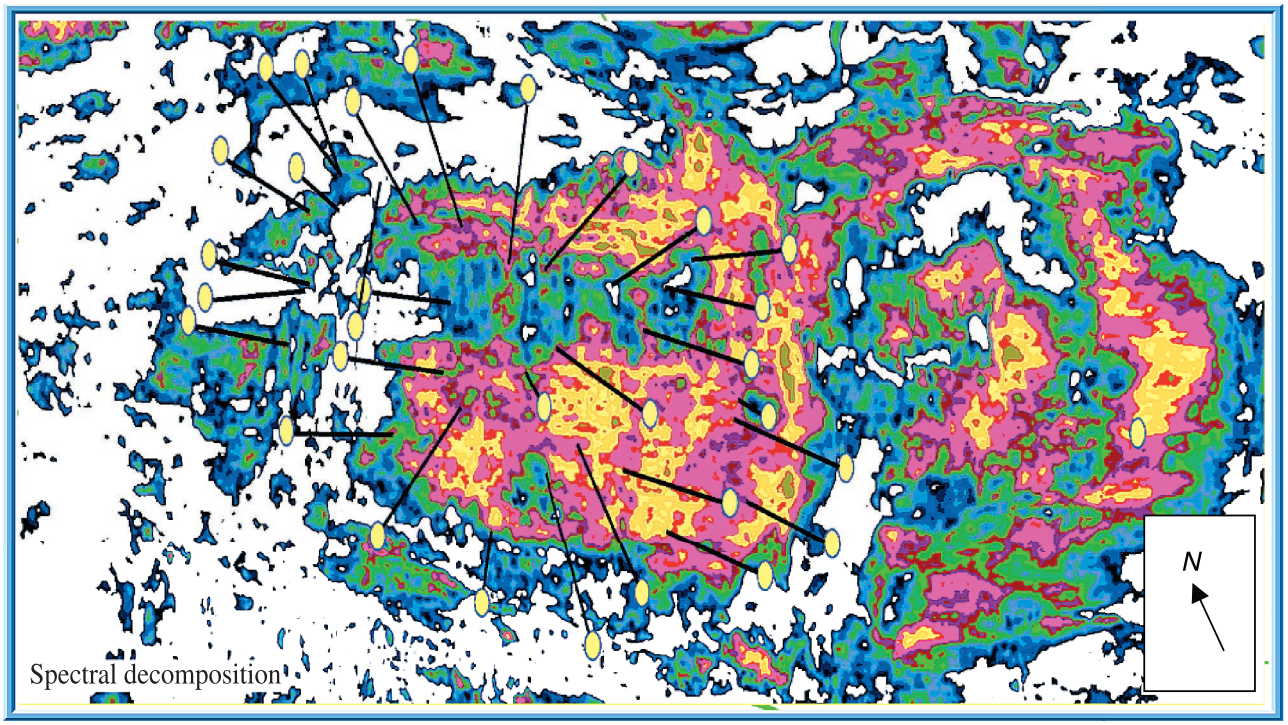

FIGURE 13. Spectral decomposition attribute map of the B Zone of the Liuhua reservoir. A lack of contiguous acoustic resonance (white and blue colors) in the western field area is interpreted as reduced porosity resulting from the destruction of continuity in trace-to-trace similarity. Spectral decomposition attribute is indicative of primary matrix competence, which in the case of Liuhua field is probably a primary depositional, facies-dependent parameter, modified during karsting and carbonate dissolution.

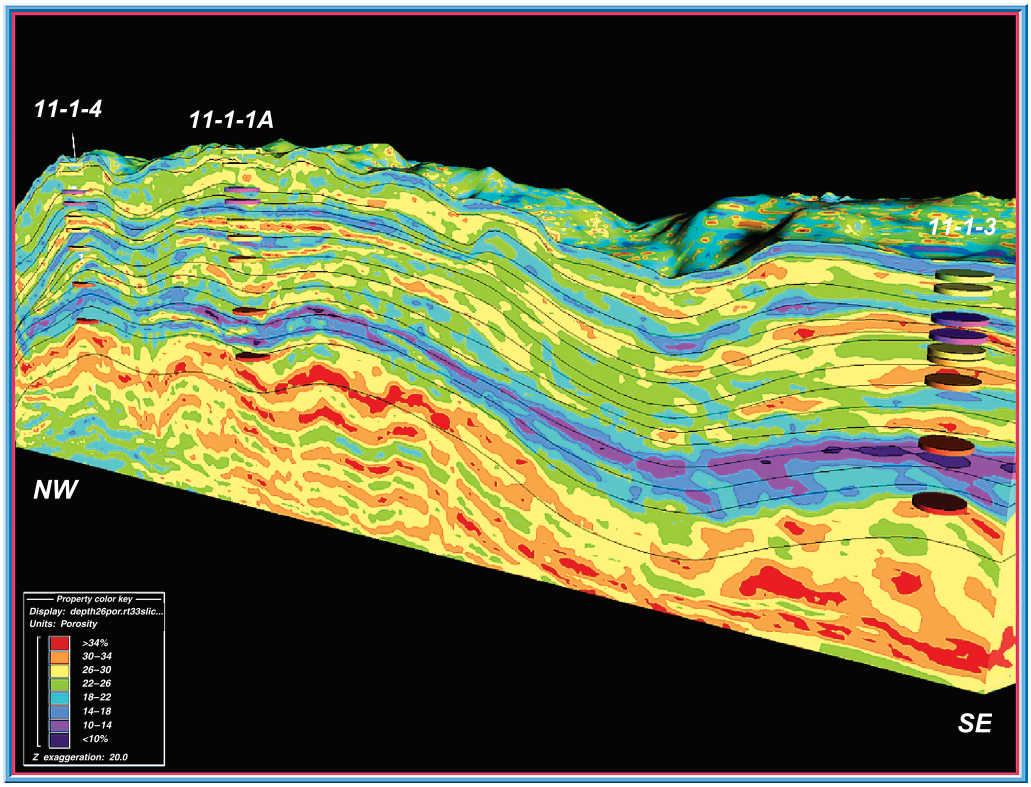

FIGURE 14. Porosity volume of Liuhua field cut along a northwest-southeast cross section. This orientation along the long axis of the reservoir shows tops of internal reservoir zones (black lines) picked from seismic, tops from vertical wellbores LH 11-1-4, LH 11-1-1A, and LH 11-1-3 (disks), and porosity calculated from inversion of acoustic impedance using core-calibrated porosity values (coloring). Zones of high porosity are shown in red, whereas zones of low porosity are shown in blue. Vertical exaggeration = 20. Note the linear but discontinuous zones of alternating high and low porosity. Extracted low-porosity volumes colored blue and violet are shown in Figure 16.

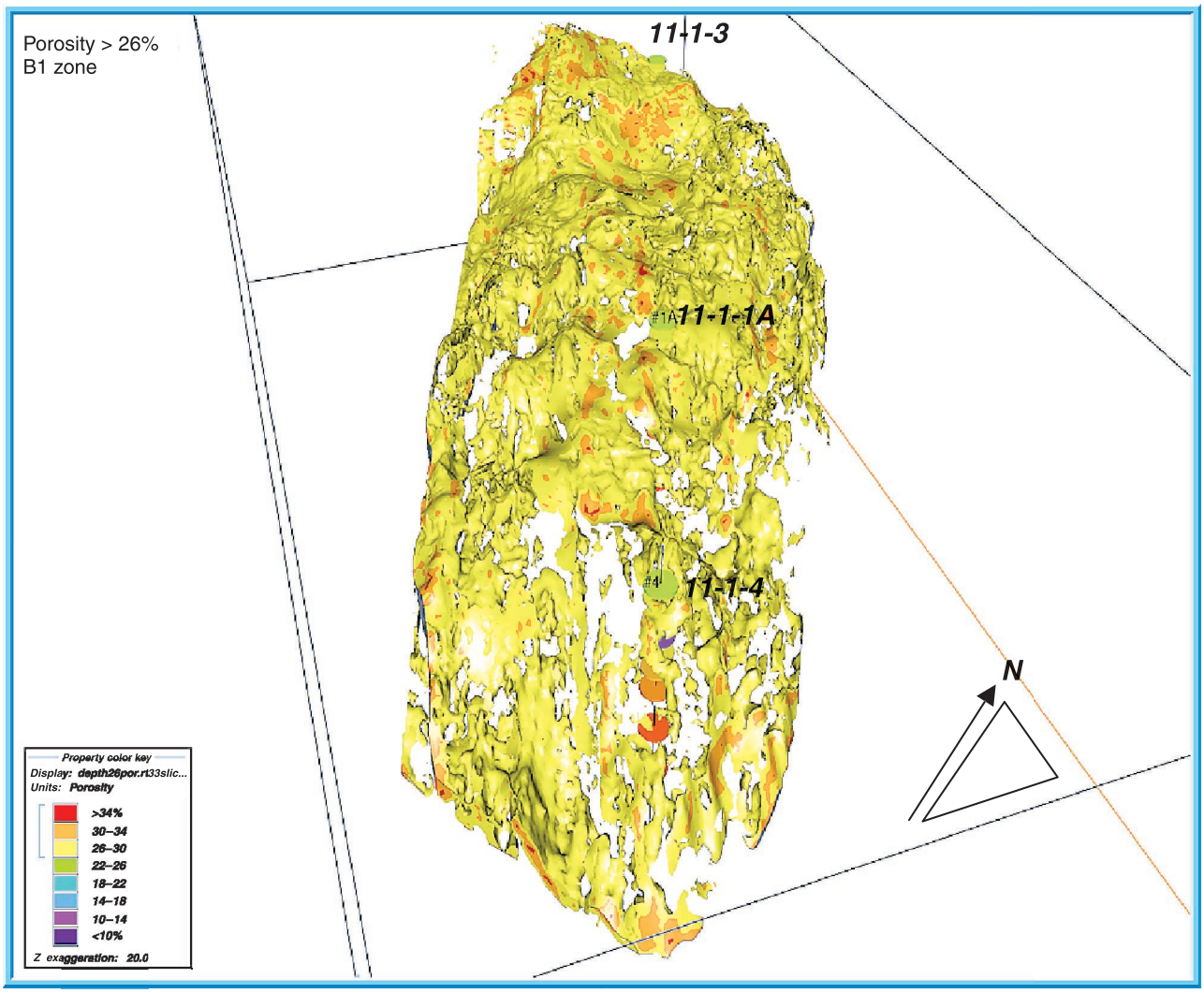

FIGURE 15. Extracted reservoir volume showing only porosity values greater than 26% (high-quality reservoir) from the topmost and most densely drilled producing zone, B1. View is from northwest to southeast, similar to the viewpoint of Figure 7. Location and tops of the three vertical wells LH 11-1-4 (foreground), LH 11-1-1A (middle ground), and LH 11-1-3 (background) are shown as green disks. Images of this kind are useful to assess fieldwide porosity or tightness of individual reservoir zones. The penetration of continuous zones of high porosity by production wellbores is a critical prerequisite for high flow rates and economic well lifespan. Note the more contiguous and slightly higher porosity in the southeastern part of the field (background), contrasting with the ''patchy'' distribution of high-quality reservoir in the foreground. Reduction in porosity there is probably associated with physical collapse of porous carbonate framework through faulting and dissolution, stylolitization, increased cementation along selected faults, and reduced effectiveness of diagenetic dissolution processes.

depth-converted porosity data calculated from seismic data; this served as a critical quality check of the conversion accuracy.

The reservoir porosity characterization allows the display of contoured porosity volumes, either associated with specific zones or with defined porosity value intervals to visualize regional distribution or the degree of tightness of individual reservoir zones (Figures 15, 16). The extracted volume of high-quality reservoir (>26% porosity) within the main target horizon indicates that high porosity is reasonably continuous in the central development area and the southeastern, undeveloped extension area. Stratification in the western area, however, which is accessed by several development wells, is considerably more discontinuous than originally anticipated because of porosity heterogeneity. The extent of the ''low-porosity'' zones (<14% porosity, Figure 16) is far from continuous, illustrating the major production problem of Liuhua field: There are no contiguous aquitards to protect the topset wellbores from early water breakthrough. The results demonstrate that Liuhua reservoir is not a simply stratified stack of alternating tight and porous strata, as envisioned in the original development plan. Rather, the principal low-porosity zones

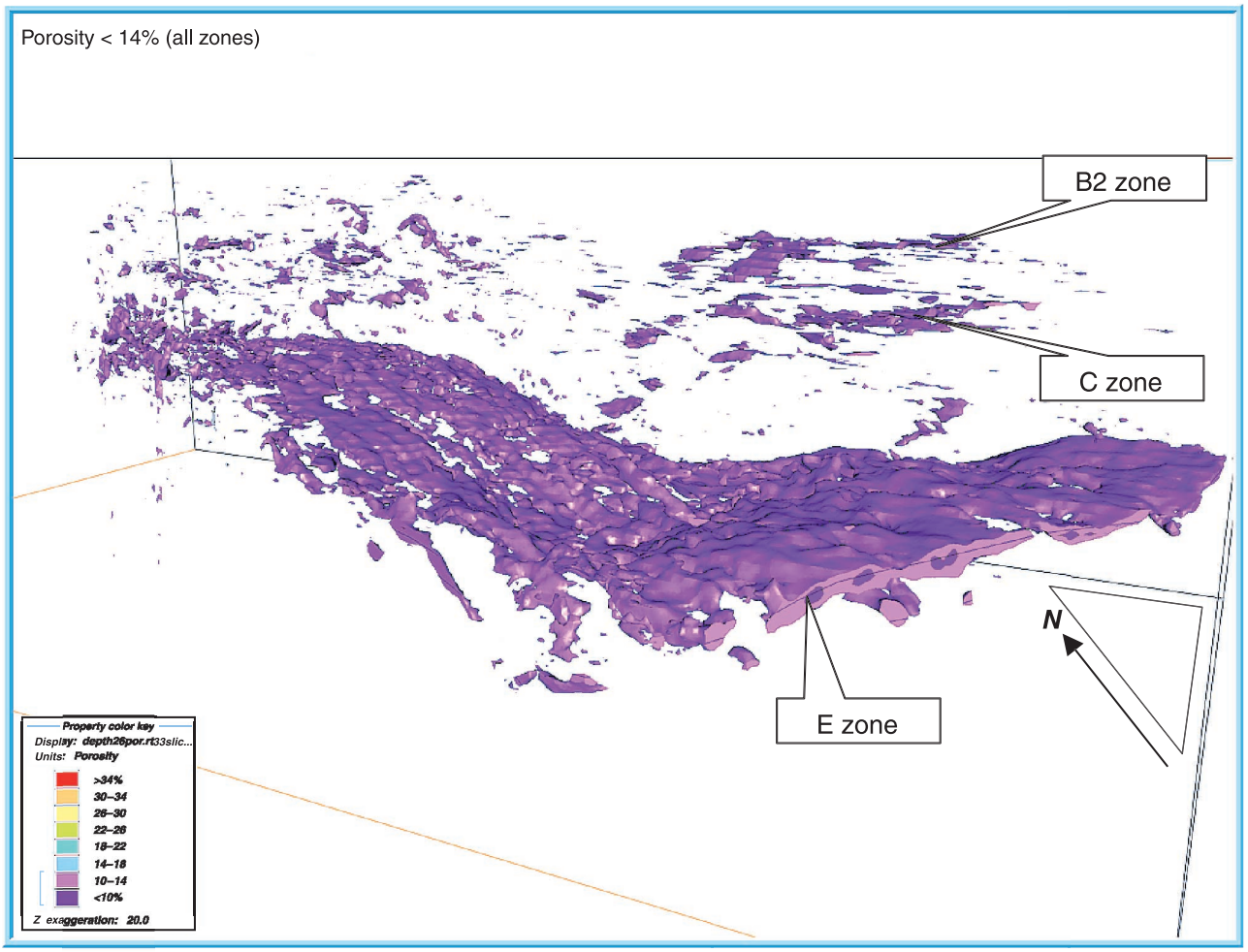

FIGURE 16. Partial volume extracted from porosity volume of Figure 14, showing only porosity values less than 14% (''tight'' zones) from all zones of Liuhua. The volume displays the high variability in thickness and continuity of low-porosity zones within the reservoir. The original assumption of fieldwide continuity for tight zones is met only for E Zone. However, this zone dips below the OWC at the field margins and in the gentle syncline in the middle foreground. It therefore offers only limited wellbore protection against premature water breakthrough. Structurally higher low-porosity zones (C, B2) are highly discontinuous.

(C, E) are penetrated by numerous gaps of high porosity. Overall, stratigraphic discontinuity of the low porosity zones (principally C, but also B2 and, in places, E) resulting from any of the processes discussed above will greatly weaken their role of protecting the topset production wellbores (mostly in B1) from early water breakthrough.

RESERVOIR SIMULATION

A final reservoir simulation model honored the geoscience reservoir model. The zonal-porosity averages for all 14 units in the reservoir characterization model were transferred directly into the simulator. The geologic correlations and petrophysical rock-type modeling were incorporated with permeability values calculated from porosity and integrated with water saturation values in a depth-converted porosity model. This integration allowed the definition of petrophysical rock types and hydraulic flow units. For simulation purposes, the original structure and porosity model, which had been gridded at 75′ by 75′ horizontally by 5′ vertically, was upscaled to reach an acceptable maximum number of grid cells for the reservoir simulator while still adequately representing the internal reservoir heterogeneity. This required a 3- to 10-fold reduction in vertical resolution. The final simulation model used 15 layers to represent internal reservoir geometry and fluid distribution, with the lowest two layers representing the aquifer. Overall, the model comprised 89,100 grid blocks (Figure 17).

Permeability and water saturation were calculated by regressing core porosity vs. core permeability (Figure 18) and log-calculated effective porosity vs. log-calculated water saturation. Steady-state measurements on 16 core

plugs provided data for relative permeability. The simulation model used four different relative permeability curves representing four petrophysical rock types. The model calculated the rock type of each grid block based on its permeability-to-porosity ratio. Thus, once the rock type was determined, the relative permeability value for the grid block could be calculated for any given water saturation.

History Matching

Even after incorporating the information from 3-D seismic data, the large scatter in the permeability-vs.-porosity relationship (Figure 18) and the unknown impact of faults and discontinuities on flow behavior imposed significant uncertainties in the reservoir description, thereby limiting the predictive ability of the reservoir model. A useful method to improve this shortcoming is history matching, in which simulated reservoir productivity is compared with historic field-wide and well-specific production performance. Reservoir parameters can then be adjusted to obtain a reasonable match. We adjusted, where necessary, vertical-to-horizontal permeability ratio, permeability value, and effective length of the wellbore. Because of the variability of the historical data caused by pump-operating conditions, temporary shut-ins, and gauge accuracy, we focused on matching the monthly average performance instead of the transient variations of data.

History matching suggests that production performance is controlled by water coning through the formation and by water channeling through faults, fractures, dissolution microfractures, and gaps in the

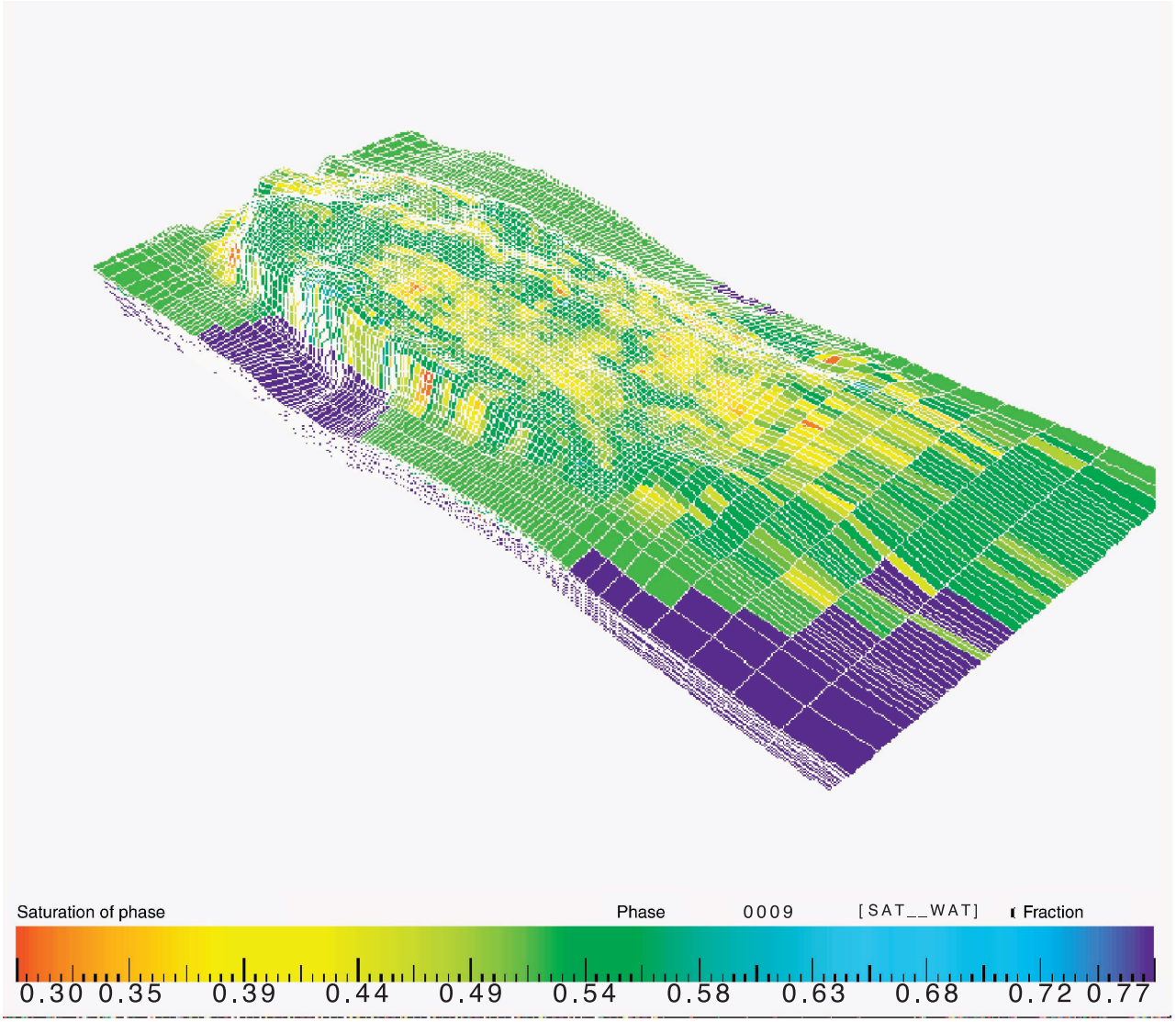

FIGURE 17. Reservoir simulation model of Liuhua field showing initial fieldwide water saturation in principal reservoir zone B1.

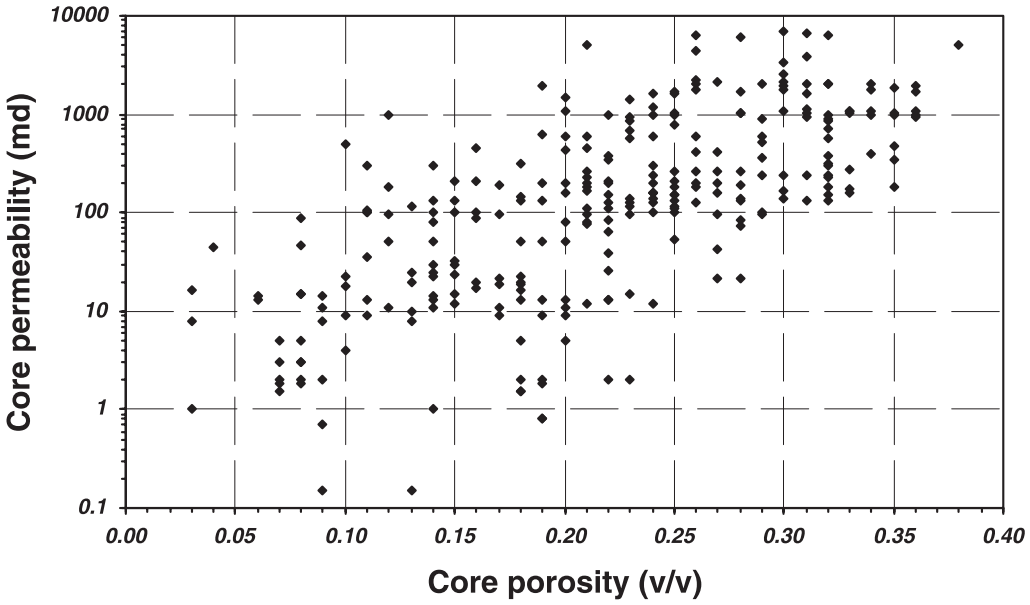

FIGURE 18. Permeability-vs.-porosity crossplot from selected plugs of the three vertical, cored wells through Liuhua field. The large scatter indicates that the rock types include a range of pore types (intergranular, intragranular, moldic, vuggy, fracture) and have experienced multiple porosity-modifying events.

low-porosity zones. The 3-D porosity model and long-term production tests support such a model. History matching also allows a model in which low-porosity zones block water coning, leaving only bounding and internal faults for water encroachment. Such a model predicts significant zones of high oil saturation and bypassed pay but is inconsistent with the bulk of the findings from the reservoir characterization. Results also indicate that uncertainties in water saturation and porosity (±5%) and horizontal permeability in the lower zones should only have a limited impact on future production performance.

Good history matches of individual well performance were achieved for a range of simulation descriptions. Modification of the geologic variables (porosity, permeability, thickness) were kept to an absolute minimum and made rapid solutions for individual well production histories possible. The reservoir characterization process, which provided high-quality detail on number and thickness of layers, fieldwide binned porosity, permeability, and water-saturation data constrained the history-matching process considerably so that the combined characterization and simulation process took ultimately significantly less time than would have been required without a reservoir characterization.

CONCLUSIONS

The very high resolution of the 3-D seismic data revealed a degree of insight into small-scale stratification and internal heterogeneity that is normally unattainable for most reservoirs. Detailed images of carbonate-collapse zones, high-resolution porosity stratification, and 2- to 4-m offsets on minor faults became readily visible. Major faults are surrounded by a halo of minor faults that accommodate both normal and strike-slip displacement along en echelon sets and that may have major impact on well productivity and reservoir fluid flow. Diffuse carbonate solution, microbreccia formation, and gas chimneys were found to be important factors affecting reservoir hydraulics. Even the 4-m resolution attained by this survey could not unequivocally identify the nature of amplitude "dim zones" associated with high water production; it is likely that these represent zones of incipient carbonate collapse. As a result of the high-resolution reservoir characterization, much of the prior geological and geophysical understanding of the reservoir was revised significantly.

In the Liuhua reservoir, the shallow, low-relief trap combined with heavy oil under strong water drive made the high-precision characterization an economic necessity. Similar high-resolution surveys for other reservoirs will likely bring out surprises that will allow improvements in reservoir management through extended field life, sustained production increase, or reduced costs. Our results suggest that significant aspects of reservoir characteristics may be missed in surveys of lower resolution.

ACKNOWLEDGMENTS

This work was performed while the first four authors were with Amoco (now BP), Houston, Texas. The authors would like to thank the management of BP Amoco, Kerr McGee, and China National Offshore Oil for permission to publish this work. Shane Pelecnaty, Gregor Eberli, and Mike Grammer improved the manuscript through helpful reviews. The senior author

thanks Mrs. Britta Ernst and Mrs. Martina Grundmann for help with the figures.

REFERENCES CITED

Bourrouilh, L. J. F. G., 1998, The role of high-energy events (hurricanes and/or tsunamis) in the sedimentation, diagenesis and karst initiation of tropical shallow water carbonate platforms and atolls: Sedimentary Geology, v. 118, p. 3–36.

Boutell, R. D., and E. P. Moldovanyi, 1992, Sedimentology and diagenesis of the Miocene Liuhua carbonate platform, Pearl River Mouth Basin, South China Sea (abs.): AAPG Annual Meeting Program, v. 1, p. 12.

Christian, H. E., Jr., and W. W. Tyrrell Jr., 1991, Exploration history of the Liuhua 11-1-1A discovery, Pearl River Mouth Basin, China: Proceedings, Offshore Technology Conference, v. 23, p. 93–100.

Cocozza, T., and A. Gandin, 1990, Carbonate deposition during early rifting: The Cambrian of Sardinia and the Triassic–Jurassic of Tuscany, Italy, *in* M. E. Tucker, J. L. Wilson, P. D. Crevello, J. R. Sarg, and F. Read, eds., Carbonate facies: International Association of Sedimentologists Special Publication 9, p. 9–38.

Dorobek, S. L., 1997, Miocene carbonate platforms of the South China Sea region: Tectonic controls on platform inception and termination (abs.): AAPG Annual Meeting Program, v. 6, p. A29.

Erlich, R. N., S. F. Barrett, and B. J. Guo, 1990, Seismic and geologic characteristics of drowning events on carbonate platforms: AAPG Bulletin, v. 74, p. 523–1537.

Erlich, R. N., S. F. Barrett, and B. J. Guo, 1991, Drowning events on carbonate platforms: A key to hydrocarbon entrapment?: Proceedings, Offshore Technology Conference, v. 23, p. 101–112.

Erlich, R. N., A. P. Longo Jr., and S. Hyare, 1993, Response of carbonate platform margins to drowning: Evidence of environmental collapse, *in* R. G. Loucks and J. F. Sarg, eds., Carbonate sequence stratigraphy: Recent developments and application: AAPG Memoir 57, p. 241–266.

Fulthorpe, C. S., and S. O. Schlanger, 1989, Paleooceanographic and tectonic settings of early Miocene reefs and associated carbonates of offshore Southeast Asia: AAPG Bulletin, v. 73, p. 729–756.

Gascoyne, M., G. J. Benjamin, H. P. Schwarcz, and D. C. Ford, 1979, Sea-level lowering during the Illinoian glaciation: Evidence from a Bahama ''blue hole'': Science, v. 205, p. 806–808.

Gu, K. J., and Y. Q. Ye, 1992, Tests verify advantages of horizontal well in offshore China oil field: Oil & Gas Journal, v. 90, (42), Oct. 19, 1992, p. 76–80.

Heubeck, C., P. Peng, C. Story, and Z. J. Yuan, 1998, Detailed carbonate stratigraphy from log interpretation of horizontal wells assists in reservoir management (Liuhua field, offshore China) (abs.): AAPG Annual Meeting Program and Extended Abstracts, v. 1, p. A295.

Hill, C. A., 1992, Sulfuric acid oil-field karst, *in* M. P. Candelaria and C. L. Reed, eds., Paleokarst, karst-related diagenesis, and reservoir development: Examples from Ordovician–Devonian age strata of west Texas and the Mid-Continent: SEPM, Permian Basin Chapter Publication 92-33, p. 192–194.

Hill, C. A., 1995, H_2S-related porosity and sulfuric acid oil-field karst, *in* D. A. Budd, A. H. Saller, and P. M. Harris, eds., Unconformities and porosity in carbonate strata: AAPG Memoir 63, p. 301–306.

James, N. P., and P. W. Choquette, 1990, The meteoric diagenetic environment, *in* I. A. McIlreath and D. W. Morrow, eds., Diagenesis: Geoscience Canada Reprint Series 4, p. 35–74.

Kerans, C., 1988, Karst-controlled reservoir heterogeneity in Ellenburger Group carbonates of west Texas: AAPG Bulletin, v. 72, p. 1160–1183.

Loucks, R. G., 1999, Paleocave carbonate reservoirs: Origins, burial-depth modifications, spatial complexity, and reservoir implications: Journal of Sedimentary Research, v. 83, p. 1795–1834.

McMechan, G. A., R. G. Loucks, X. X. Zeng, and P. Mescher, 1998, Ground penetrating radar imaging of a collapsed paleocave system in the Ellenburger dolomite, central Texas: Journal of Applied Geophysics, v. 39, p. 1–10.

Moldovanyi, E. P., F. M. Wall, and J. Y. Zhang, 1995, Regional exposure events and platform evolution of the Zhujiang Formation carbonates, Pearl River Mouth Basin: Evidence from primary and diagenetic seismic facies, *in* D. A. Budd, A. H. Saller, and P. M. Harris, eds., Unconformities and porosity in carbonate strata: AAPG Memoir 63, p. 125–140.

Mylroie, J. E., and J. L. Carew, 1995, Geology and karst geomorphology of San Salvador Island, Bahamas: Carbonates and Evaporites, v. 10, p. 293–206.

Purdy, E. G., and G. T. Bertram, 1993, Carbonate concepts from the Maldives, Indian Ocean: AAPG Studies in Geology 34, p. 1–56.

Stark, P. H., 1991, Horizontal drilling: Overview of geologic aspects and opportunities: AAPG Bulletin, v. 75, p. 1399.

Tinker, S. W., and D. H. Hruk, 1995, Reservoir characterization of a Permian giant: Yates field, west Texas, *in* E. L. Stoudt and P. M. Harris, eds., Hydrocarbon reservoir characterization: Geologic framework and flow unit modeling: SEPM Short Course Notes, p. 51–128.

Turner, N. L., 1990, The lower Miocene Liuhua carbonate reservoir, Pearl River Mouth Basin, offshore People's Republic of China (abs.): AAPG Bulletin, v. 74, p. 1006–1007.

Turner, N. L., and P. Z. Hu, 1990, The lower Miocene Liuhua carbonate reservoir, Pearl River Mouth Basin, offshore People's Republic of China: AAPG Bulletin, v. 74, p. 781.

Turner, N. L., and P. Z. Hu, 1991, The lower Miocene Liuhua carbonate reservoir, Pearl River Mouth Basin, offshore People's Republic of China: Proceedings, Offshore Technology Conference, v. 23, p. 113–123.

Tyrrell, W. W., Jr., and H. E. Christian, 1992, Exploration history of the Liuhua 11-1-1A Miocene carbonate

discovery, Pearl River Mouth Basin, China: AAPG Bulletin, v. 76, p. 1209–1223.

Wagner, P. D., D. R. Tasker, and G. P. Wahlman, 1995, Reservoir degradation and compartmentalization below subaerial unconformities: Limestone examples from west Texas, China, and Oman, *in* D. A. Budd, A. H. Saller, and P. M. Harris, eds., Unconformities and porosity in carbonate strata: AAPG Memoir 63, p. 177–194.

Wu, X. C., P. H. Li, and P. Z. Hu, 1997, Reservoirs of chalkified Miocene reef-banks on Dongsha Platform in South China Sea, *in* Z. C. Sun, T. B. Wang, D. L. Ye, and G. J. Song, eds., Proceedings of the 30th International Geological Congress 18A, p. 239–253.